



Enhancing nanofiltration in thin film nanocomposite membranes using Bi-Metal modified biochar nanofillers

Mahesan Naidu Subramaniam^a, Shouyong Zhou^b, Guangru Zhang^{c,d}, Jinesh C. Manayil^a, Zhentao Wu^{a,*}

^a Energy and Bioproducts Research Institute, Aston University, Aston St, Birmingham B4 7ET, UK

^b Jiangsu Engineering Laboratory for Environmental Functional Materials, Jiangsu Key Laboratory for Biomass-based Energy and Enzyme Technology, School of Chemistry and Chemical Engineering, Huaiyin Normal University, No. 111 West Changjiang Road, Huaian 223300, Jiangsu Province, PR China

^c State Key Laboratory of Materials-Oriented Chemical Engineering, College of Chemical Engineering, Nanjing Tech University, 30 Puzhu Road(S), Nanjing 211816, PR China

^d Quzhou Membrane Material Innovation Institute, Nanjing Tech University Quzhou, 99 Zheda Rd, Quzhou 324000, PR China

ARTICLE INFO

Editor: V Tarabara

Keywords:

Biochar nanofiller
Thin-film nanocomposite
Interfacial polymerisation
Methylene orange, desalination

ABSTRACT

The advancement in the development of nanofillers for thin-film nanocomposite (TFN) membranes, particularly those derived from eco-friendly sources, has gained increasing recognition. This is largely due to their potential to markedly improve both permeation and selectivity. However, the investigation of biochar (BC), a by-product of biomass pyrolysis, as a distinctive nanofiller remains limited. This study investigates the incorporation of porous iron/zinc (Fe/Zn) modified biochar (MBC) into a polyamide active layer for the purpose of fabricating TFN membranes on a polyethersulfone (PES) substrate via interfacial polymerisation (IP). Imaging confirmed the formation of metal nanoparticles dispersed uniformly throughout the porous BC substrate. Further crystallinity and surface analysis suggest strong interactions between metal and BC substrate, with a surface area of 117.99 m²/g and high nanofiller pore volume of 7.72 cm³/g. The effects of incorporating MBC into both the membrane substrate and polyamide (PA) layers on the physicochemical properties, permeation, and rejection of salts and dye were examined. Scanning Electron Microscopy (SEM) imaging has shown that the incorporation of MBC in both the substrate and PA layer results in the seamless formation of a finger-like structure spanning both layers. This incorporation also causes a minor increase in the surface roughness of the PA layer. Fourier transform Infra-Red (FT-IR) spectroscopy shows an enhancement in hydrophilic functional groups (-OH and -COOH) on the membrane surface, as evidenced by the reduced contact angle value of 55°. Permeation and rejection testing indicate that M5, where MBC was incorporated in both substrate and thin film structure, was the best performing membrane, with water permeance from the feeds of water, MO, MgSO₄ and NaCl solutions of 46.55 ± 0.08, 44.49 ± 0.28, 37.43 ± 0.36, and 21.55 ± 0.03 Lm²h⁻¹bar⁻¹, respectively. Rejection of MO, MgSO₄ and NaCl were recorded to be 99.53 ± 0.02, 99.25 ± 0.09 and 46.99 ± 0.69 %. This study provides a compelling perspective on the application of green-derived BC as a nanofiller in the fabrication of TFN membranes for desalination, resulting in enhanced water product quality.

1. Introduction

The need for clean water has surpassed its availability, with approximately 25 % of the world's population living in regions experiencing varying degrees of water stress. [1]. This situation is expected to deteriorate in the coming decades due to factors such as a rapid increase in demand, ongoing population growth, and climate change [2,3]. Desalination is recognised as a vital solution for addressing the global

water scarcity, and the recovery of potable water from non-freshwater sources like seawater or brackish water has been seen as a feasible and sustainable solution [3,4]. Meanwhile, there is an urgent need for cost-effective, energy-efficient, and low-carbon technologies to reclaim such water. As a result, membrane technology is able to attract significant research interest due to advantages such as the high separating selectivity, permeability, low operational cost, and modular designs for a wide range of applications [5–7]. While there are two types of common

* Corresponding author.

E-mail address: 3z.wu7@aston.ac.uk (Z. Wu).

<https://doi.org/10.1016/j.seppur.2024.128236>

Received 26 February 2024; Received in revised form 29 May 2024; Accepted 30 May 2024

Available online 31 May 2024

1383-5866/© 2024 The Authors. Published by Elsevier B.V. This is an open access article under the CC BY license (<http://creativecommons.org/licenses/by/4.0/>).

membranes for water treatment, namely polymeric (organic) and ceramic membranes, the latter tends to be more expensive despite offering superior mechanical and chemical durability. Therefore, polymeric membranes, especially thin film composite (TFC) membranes offering both high water permeation and selectivity, have been developed and are receiving continuously increasing research interest.

Over the years, a range of modification techniques have been utilized by researchers to enhance the permeability and selectivity of TFC membranes. These methods encompass the incorporation of hydrophilic materials, plasma treatment, blending with functional nanomaterials, UV irradiation, and more [8–10]. Among these techniques, the employment of functional nanofillers has shown considerable potential. This is attributed to several advantages including a simple modification process, superior performance, cost efficiency, and easy reproducibility. Various forms of nanomaterials, such as metals (titania, copper, silver) [11,12], non-metals (graphene oxide, carbon nanotubes) [13,14], and composites (graphene-titania, carbon-nanotube-silver, metal-carbon dots) [15,16], have been integrated into TFC membranes to enhance separation performance. Meanwhile, certain inherent characteristics are sought before these nanofillers are incorporated into the membranes. These characteristics encompass hydrophilic functional groups, a substantial surface area, porous structures to aid water transport, and a charged nature to enhance ion repulsion. [17]. When incorporated into the polymeric membranes via processes like interfacial polymerisation (IP), these inherent characteristics serve to enhance permeation and selectivity of the membranes during wastewater treatment [18]. Zhao et al. [19] utilised the IP process to integrate UiO-66-NH₂ nanoparticles into the thin film membrane. The goal was to enhance the membrane selectivity at a molecular level, which subsequently enhanced the permeation and rejection capabilities of the membrane for different salts found in brackish water. Similarly, Konsowa et al. [20] utilised titanium dioxide (TiO₂) nanoparticles to prepare a TFC membrane for forward osmosis (FO) application. The use of 0.5 wt% of the nanoparticle significantly increased the porosity and hydrophilicity of the membrane, resulting in a twofold improvement in permeation and separation.

Carbon-based materials, such as graphene and carbon nanotubes, form an important family of nanofillers. However, they typically require specialised material processing techniques that involve the use of chemicals and solvents. In contrast, biochar (BC), a bio-based material produced as a by-product of biomass pyrolysis in the generation of biogas and biofuel, has been underutilised. The current application of BC is primarily focused on soil remediation in the agricultural sector [21]. Nevertheless, BC exhibits several characteristics that make it suitable as a nanofiller in polymeric membranes, including a highly porous network, the presence of hydrophilic functional groups, and a high surface area. Zhang et al [22] integrated ball-milled BC into a TFN (thin film nanocomposite) membrane for the purpose of separating tetracycline antibiotics from wastewater. The authors hypothesised that the ultrafine size of BC, along with its high porosity, facilitated the uniform dispersion of the nanofiller throughout the TFN matrix, thereby improving water transport capabilities. Furthermore, the integration of bimetal nanoparticles into the porous network of BC would enhance the membrane's water transport capability by creating a greater number of water transport channels throughout the membrane [23]. Additionally, the inclusion of Fe and Zn into the membrane has consistently demonstrated a positive effect on the membrane's hydrophilicity, enhanced the membrane's antifouling capabilities, and improved the adsorption of pollutants present in various wastewater streams. [24,25].

As a result, BC, derived from the pyrolysis of wheat straw (WS), has been functionalised with the bi-metal of Fe-Zn in this study to produce a modified biochar (MBC). The MBC was then used as the nanofiller and incorporated into both the selective layer and the porous poly-ethersulfone (PES) substrate of a TFN nanofiltration membrane. The objective is to enhance the permeation and selectivity of water separation from various sources, including seawater and textile industry wastewater. The MBC was characterised using scanning electron

microscopy (SEM), transmission electron microscopy (TEM), X-ray Diffraction (XRD), and surface area analysis. Subsequently, the prepared TFN membranes were examined using different characterisation techniques, including SEM, electron dispersion spectroscopy (EDS), Fourier transform infrared spectroscopy (FT-IR), water contact angle, and atomic force microscopy (AFM). To comprehend the effects of the MBC on the separation performance of the prepared TFN membranes, tests for pure water permeation, salt rejection, and dye rejection were conducted. This work is expected to provide meaningful insight into the use of greener materials, such as BC, as sustainable nanofillers to enhance the separation performance of state-of-the-art polymeric membranes.

2. Methodology

2.1. Reagents and chemicals

PES was utilised to prepare the membrane support layer (Sigma Aldrich, MW 58 K). Piperazine (PIP, 99 %), 1,3,5-benzenetricarbonyl trichloride (TMC, 98 %), n-hexane (97 %), n-methyl-2-pyrrolidone (NMP, 99 %), polyvinylidene pyrrolidone (PVP) K360 (99 %), methylene orange (MO), sodium chloride (NaCl, 99 %) and magnesium sulphate (MgSO₄, 99 %) were all procured from Sigma Aldrich. All the reagents employed in this study were used without any alterations. They were dissolved in MilliQ ultrapure water for usage, unless stated otherwise.

2.2. Preparation and characterisation of the MBC filler

WS pellets (7 mm OD and approximately 12 mm long) were used as raw feedstock for the preparation of BC. The WS pellets were manufactured without using any binder. The as-received biomass was directly pyrolyzed (500 °C, N₂ atmosphere, 120 min) without any preliminary milling step. The BC collected was then cooled to room temperature (23 °C), rinsed with ultrapure water, dried at 80 °C, and ground using an agate mortar before being sieved using a 300-mesh filter.

The BC was subsequently modified by metallic nanoparticles, specifically iron (Fe) and zinc (Zn). A straightforward co-precipitation technique, which has been detailed elsewhere, was employed for this purpose [26]. In a typical process, 25 mL of aqueous 0.4 M Fe (NO₃)₃·9H₂O and 25 mL of aqueous 0.2 M and Zn(NO₃)₂·6H₂O were prepared separately before being mixed in a beaker of 100 mL in volume. The molar ratio between Fe and Zn was kept at 2:1 [27]. This was followed by the addition of 1.5 g of the BC, keeping the total metal component in each MBC at 0.6 M. The pH of the solution was maintained at 12 through dropwise additions of 6 M NaOH. The mixture was then heated to 80 °C and maintained at this temperature for 1 h at a constant stirring rate of 250 rpm. The mixture was then cooled to room temperature. The precipitate formed was collected and rinsed with ultrapure water to remove residual ions, prior to be dried at 100 °C for 24 h and grounded into powder using a pestle and mortar. The final samples were calcined at 500 °C for 2 h at a ramping rate of 5 °C/min under a nitrogen (N₂) atmosphere. Characterisations such as morphology, dispersion, functional group, crystallinity, surface area, and surface charge were carried out via transmission electron microscopy (TEM, HT 7700, Hitachi), energy-dispersive x-ray spectroscopy (EDS, Oxford Instruments 400), Fourier transform-infrared spectroscopy (FT-IR, Thermo Scientific Nicolet iS50 Spectrometer), x-ray diffraction (XRD, Bruker D8 Advance), Brunnaur-Emmett-Teller (BET, Quantachrome Nova 4000e) analysis, nanofiller dispersion stability test, and zeta potential (Malvern Zetasizer Nano ZSP).

2.3. Fabrication of the PES membrane substrate

The PES membrane substrates were fabricated via a non-solvent induced phase inversion process, details of which can be found elsewhere [13]. For the preparation of the unmodified substrate membrane

(neat PES membrane), a homogeneous polymer casting solution was formed by dissolving 1 wt% of PVP K30 and subsequently 20 wt% PES in NMP. The solution was stirred at 50 °C for 24 h until it became uniform. For the preparation of a mixed matrix membrane (MMM) substrate layer, 1 wt% of MBC was first added into the NMP, sonicated for 60 min, before subsequently adding both 1 wt% of PVP K30 and 20 wt% PES, and stirred under the same conditions until a homogeneous polymer solution was obtained. The prepared solutions were first allowed to cool down to room temperature, and subsequently placed into an ultrasonicator for 60 min to remove any trapped air bubbles (degassing). After degassing was completed, the solution was poured onto a glass plate and the membranes were cast using a glass rod. After the casting process, the glass plate, which held the cast polymer film, was immersed in ultrapure water to induce phase inversion. This was done after a lapse of 15 s. The membranes, once prepared, were immersed for a duration of 24 h. The water was replaced every 12 h to facilitate the completion of the solvent removal process. Following this, the membranes were stored in DI water until they were needed for further use or processing.

2.4. Fabrication and characterisation of the PA separating layer

A polyamide (PA) separating layer was formed on the surface of the porous PES substrate, with or without the MBC, through an IP process using PIP and TMC. In a typical process, an aqueous solution of PIP (2 w/v%) was applied to the PES substrate surface and left for 2 min. The excess solution was then removed using a rubber roller and dried in the oven for 20 s. Subsequently, a TMC solution (0.1 w/v%), dissolved in n-hexane, was applied to the same surface, and left for 20 s before the excess solution was removed. The TFC and TFN membranes obtained were then placed in an oven at 80 °C for 10 min to complete the IP process, before being stored in ultrapure water. For membranes with MBC embedded on the thin film, the MBC was dispersed in the TMC solution (0.1 w/v%). TMC incorporated with MBC were sonicated for 30 min before being used before TFN preparation. Fig. 1 provides a graphical overview of the IP process.

In this study, we investigated the impact of incorporating MBC into different structures of the membrane, specifically the selective PA layer and the substrate (PES). We prepared five distinct membranes: M1 (without PA layer or MBC), M2 (without MBC), M3 (MBC in PA layer), M4 (MBC in substrate), and M5 (MBC in both substrate and PA layer). A summary of the membranes prepared in this study can be found in Table 1.

The membranes prepared in this study were analysed for their characteristics, including the surface morphology, cross-section morphology, surface roughness, porosity, water contact angle, surface

Table 1

Summary of the membranes prepared in this work.

Membranes	Denomination	Presence of nanofiller	MBC loading (wt. %)
Neat	M1	None	0
Neat-TFC	M2	None	0
Neat-TFN	M3	Selective PA layer	0.1
MMM-TFC	M4	Substrate PES layer	1
MMM-TFN	M5	Substrate and selective PA layer	1 and 0.1

functional groups, and thermal stability. The apparent porosity of the membranes was calculated using Eq (1) [28,29]:

$$\varepsilon = \frac{W0 - W1}{V} \times 100\% \quad (1)$$

where ε is the apparent membrane porosity, $W0$ and $W1$ is the weight of wet and dry membrane in grams, respectively, and V is the membrane volume in cm^3 .

2.5. Batch filtration tests

A batch filtration test of the membranes prepared in this study was conducted using a dead-end filtration unit (Sterlitech, U.S.A). Briefly, 250 mL of ultrapure water was loaded into the testing cell and a N_2 pressure of 6 bar was applied to compact the membranes for 60 min. The effective membrane area was 14.6 cm^2 . The batch filtration test was carried out at a constant pressure of 5 bar. The volume of effluent was measured using a measuring cylinder and recorded every 10 min. The membrane permeability was calculated using Equation (2):

$$J = \frac{V_m}{A \cdot \Delta t \cdot \Delta P} \quad (2)$$

where J is the permeability of the prepared membrane ($\text{LMHB}, \text{Lm}^{-2}\text{h}^{-1}\text{bar}^{-1}$), V_m is the volume of permeate (L), A is the effective membrane area (m^2), Δt is the filtration time (h) and ΔP is the pressure used to drive the filtration process (bar). In this study, the separation performances of the prepared membranes were investigated using feed solutions of 10 ppm of MO, 1000 ppm of MgSO_4 , and 1000 ppm of NaCl. Filtration performance of the feed solution was evaluated after conducting ultrapure water filtration tests. This was done to ensure that the membranes were properly compacted prior to any filtration studies. 10 mL of permeate were collected at known intervals to investigate the solution of permeate. The concentration of the permeate solutions was evaluated using multiple instruments, including a Mettler-Toledo FiveEasy

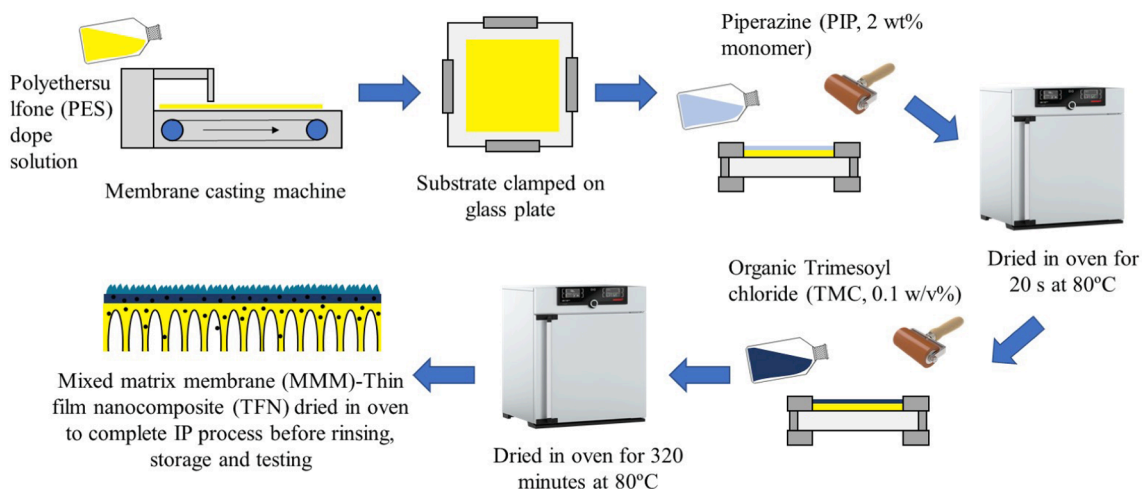


Fig. 1. Graphical overview of the IP process for preparing the thin film membranes.

Benchtop F20 pH/mv conductivity meter (for MgSO_4 and NaCl) and a Thermo Fisher Evolution 220 UV-Vis Spectrophotometer (for MO). The rejection rate of various feed solutions was calculated based on Equation (3) [30]:

$$R = \frac{C_f - C_p}{C_f} \times 100\% \quad (3)$$

where R is the rejection rate (%), C_f and C_p (mg/L) are the concentration of the feed solution and the permeate solution at given time, respectively.

2.6. Cyclic test of the membranes

The stability of the membrane was assessed by monitoring its permeation and rejection performance for all the solutions tested in this

study over four cycles. The membrane which exhibits the best performance in permeation and rejection based on the section 2.5 (M5) was selected for this test. Once a batch filtration (2 h) was completed, the membrane was cleaned with 1 M of HCl, followed by 1 M of NaOH, and finally with ultrapure water to remove any deposited foulants or residual molecules. All cleaning processes were carried out for 10 min at 25 °C under ultrasonication to gently remove the organic foulants attached onto the membrane surface. The membrane was then reinstalled into the testing module using a fresh batch of feed solution (10 ppm MO, 1000 ppm MgSO_4 , 1000 ppm NaCl).

3. Results & discussions

3.1. Characterisations of MBC

In this study, the BC used was ground and sieved through a 300-mesh

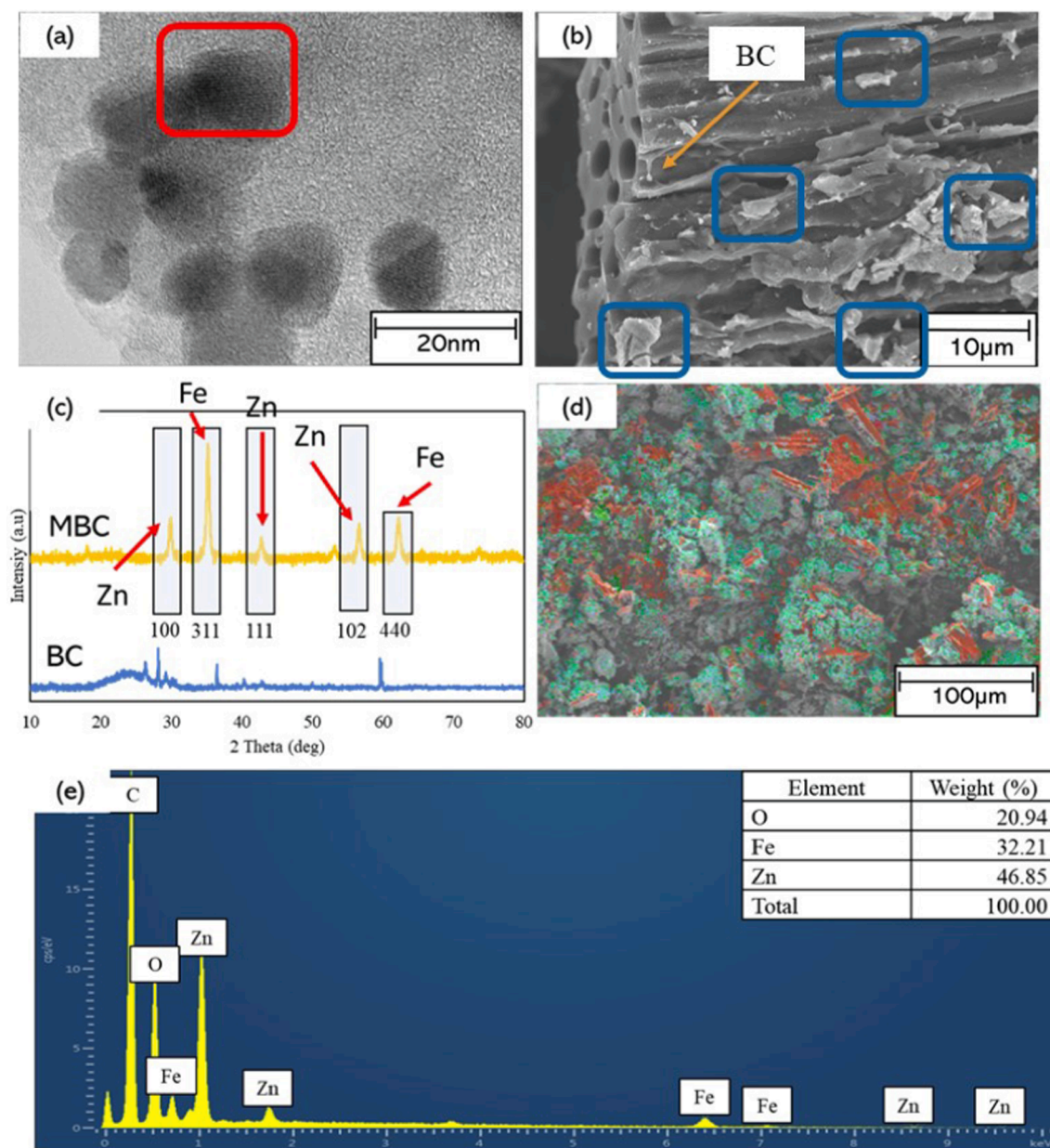


Fig. 2. Characterisations of the prepared MBC, featuring (a) TEM imaging magnified at 500 K highlighting the crystalline structure of the metal particle on the BC surface (highlighted in red), (b) SEM image of MBC with deposited nanomaterial (highlighted in blue) on surface magnified at 1.8 K, (c), XRD spectra of BC and MBC (d) EDS mapping highlighting the presence of Fe (red) and Zn (green) and (e) EDS spectra of the MBC prepared (inset: atomic weight of O, Fe, and Zn). (For interpretation of the references to colour in this figure legend, the reader is referred to the web version of this article.)

filter, before being modified with Fe and Zn nanoparticles using the co-precipitation method.

Fig. 2 (a) illustrates a detailed structural characteristic of the nano-sized metal nanoparticles deposited on the surface of BC, which are as small as less than 20 nm in diameter. Further imaging using SEM, as shown in Fig. 2 (b), unveils the presence of agglomerated particles on the BC, indicating the successful deposition of Fe and Zn nanoparticles on the bio-based substrate. The co-precipitation method is facile synthesis technique which facilitates in the development of stable composite materials, such as the deposition of Fe and Zn nanoparticles on such bio-based substrates, as evidenced here. The interaction of the metal nanoparticles with the BC was convincingly demonstrated through XRD analysis shown in Fig. 2 (c). Peaks at 29.83° (1 0 0), 35.22° (3 1 1), 39.90° (1 1 0), 53.18° (1 1 0), 59.59° (1 0 2), and 62.25° (2 0 0) (4 4 0) collectively confirm the formation of both Fe and Zn on the surface of BC (JCPDS Card No. 65–3111). Moreover, the reduction of the peak at $2\theta = 23.00^\circ$, representing the amorphous BC, implies an enhancement in the crystallinity of the BC itself. This has been corroborated in other studies that the use of a potent alkali agent (such as NaOH used in this work) can augment the crystallinity of BC, remove impurities, and enhance overall level of crystallinity [31,32]. The distribution of the metal nanoparticles on the surface of the BC is presented in Fig. 2 (d), where the EDS mapping reveals the deposition of both Fe and Zn nanoparticles with slight agglomerations. EDS spectral analysis (Fig. 2 (e)) indicates the presence of more Fe than Zn, at a ratio of 2:2.49. Despite employing a more concentrated solution for Fe at 0.4 M compared to Zn at 0.2 M during the co-precipitation process, the higher electronegativity of Zn relative to Fe can lead to a more precipitation of Zn compared to Fe. As a result, the precipitation process favoured Zn over Fe [33].

In order to comprehend the impact of metal modification on BC, particularly in terms of its interaction with water and solvent, a dispersion stability test was conducted. 0.1 w/v% of samples were added into the designated solution and sonicated for 30 min before dispersion stability test was initiated. Fig. 3 compares the dispersion stability of BC and MBC in water and NMP while Fig. 4 illustrates that.

Our findings indicate that MBC disperses well in both water and NMP. While MBC maintains its dispersion stability after 60 min, BC forms a layer and settles at the bottom of the test vial, as highlighted by the red markings in Fig. 3 (a) and (b). Both water and NMP are polar solvents, and MBC takes longer to settle compared to BC. The modification of BC with metal nanoparticles, including Fe and Zn, is crucial as it alters the surface characteristics of BC, making it more hydrophilic compared to hydrophobic BC. Hydrophobic BC experiences stronger van der Waals forces, leading to the formation of larger flocs and eventual settling, as observed in Fig. 3 (a) and (b) [34]. The metal nanoparticles on the surface of MBC allows better interaction with polar water and NMP and reduce the tendency of agglomeration between MBC

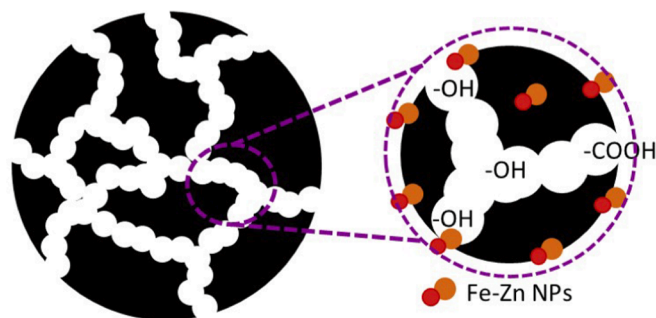


Fig. 4. Schematic illustration of incorporating Fe-Zn nanoparticles throughout the pore network of BC.

nanoparticles. Previous literature supports this observation, where hydrophilic nanoparticles (MBC) exhibit better dispersion within polar solvents such as NMP compared to hydrophobic nanomaterials (BC) [35]. The dispersion stability exhibited by MBC is an important facet in membrane preparation, as agglomeration could lead to formation of defects, leading to poor rejection performance [36]. Furthermore, good dispersion of nanofiller can lead to the formation of conformal membranes. Table 2 compares specific surface area (SSA), pore size, pore volume, and surface charge between BC and MBC.

The prepared MBC shows a significant increase in both the SSA and pore volume compared to BC, with the surface area expanding by approximately 2.5 times ($117.99 \text{ m}^2/\text{g}$) and the pore volume increasing by around 2 times ($7.72 \text{ cm}^3/\text{g}$). Meanwhile, there is a slight reduction in the pore size of the prepared MBC compared to BC. Several factors may contribute to these changes in physical properties. Firstly, the use of a potent alkali substance (6 M NaOH) in the co-precipitation process has played a significant role in exfoliating the surface and pores of the BC by removing volatile residues from the pyrolysis process [37]. Previous reports have suggested that using strong corrosive agents, such as alkali or acid, as a pre-treatment of BC before further modification can yield similar results [38]. In this case, the corrosive agent served as both an exfoliating agent and a precipitating agent for the metal nanoparticles, leading to the increase in overall pore volume the BC [39]. Meanwhile,

Table 2

Comparison of specific surface area (SSA), pore size, pore volume, and surface charge between BC and MBC.

Sample	Specific surface area (SSA, m^2/g)	Pore size (nm)	Pore volume (cm^3/g)	Zeta potential (mV)
BC	41.07	3.09	3.73	-31.13
MBC	117.99	2.72	7.72	-45.10

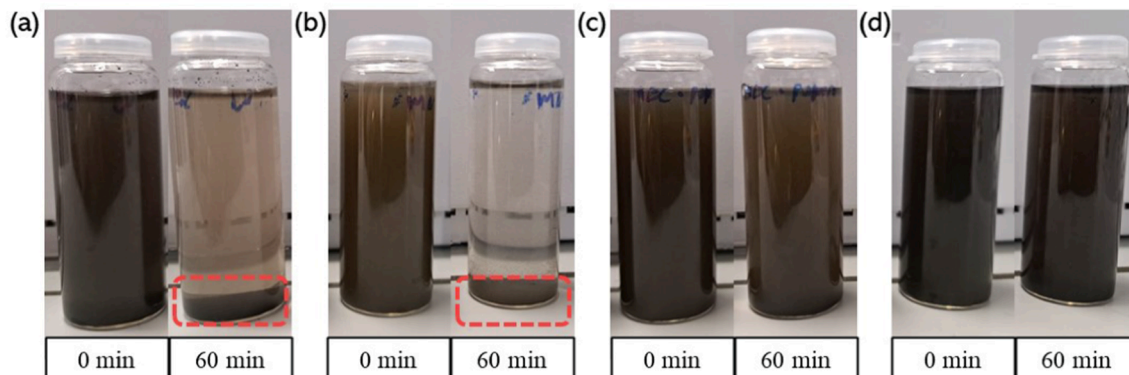


Fig. 3. Dispersion quality of 0.1 w/v% of BC and MBC at 0 min and 60 min (a) BC in ultrapure water, (b) BC in NMP, (c) MBC in ultrapure water and (d) MBC in NMP.

the precipitation of Fe and Zn nanoparticles contributed to the increased surface area of the MBC, albeit slightly. Furthermore, metal nanoparticles can enhance the hydrophilicity and consequently improve the wettability of the pores, which is synergistic in this work by benefiting the water transport of the prepared membranes [40]. However, the precipitation of metal nanoparticles can also block the pores of the BC, resulting in a reduced pore size. The zeta potential analysis reveals that the surface negativity has been amplified (from BC: -31.13 eV to MBC: -45.10 eV) due to the incorporation of metal nanoparticles, agreeing with previous research [41].

3.2. Rationales of using MBC for TFN membranes

Research has highlighted the drawbacks of carbon-based nanofillers, especially concerning the stability of particles and dispersion within polymer matrices. Noamani et al. [42] suggested that carbon nanotubes (CNT) demonstrate limited compatibility with polymer structures due to their lack of interaction with solvents like NMP and n-hexane. These solvents are frequently used in the creation of polymeric membranes and TFN. This weak adhesion of nanofillers leads to stress concentration at the polymer-nanofiller interface, potentially causing the composite to fail. However, this issue can be alleviated by modifying these nanofillers with hydrophilic composites, such as metal nanoparticles [43]. The introduction of metal composites can boost the dispersion of carbon nanofillers like BC by enhancing their stability within solvents and strengthening their interaction and compatibility with polymer matrices. The stability of nanofillers within solvent systems is vital as it reinforces the polymer matrix and improves the adhesion of TFN onto the membrane substrate [44]. Furthermore, nanofillers can aid in reducing voids and defects on membrane surfaces [45], which is advantageous for the permeation and selectivity of membranes.

The MBC developed in this study were naturally porous, boasting a high surface area of 117.99 m²/g and a substantial pore volume of 7.72 cm³/g. The deposition of Fe and Zn nanoparticles on the surface not only increased its hydrophilicity but also improved the stability of the

nanofiller in the solvent system during membrane fabrication. This stability is essential for creating a conformal and defect-free membrane. In the literature, other carbon-based materials such as carbon nanotubes, graphitic carbon nitride, and graphene are frequently used as carbon-based fillers due to their similar characteristics (porosity, high surface area, hydrophilicity) that enhance water transport through the membrane [42,46]. While these materials require highly specialised synthesis routes, BC is a by-product of biomass pyrolysis, making it a more cost-effective and sustainable option for large scale fabrication of high performance TFC membranes.

3.3. Characterisation of membranes

SEM imaging, as depicted in Fig. 5, provides a detailed perspective on the structural changes observed because of MBC integration. Cross-sectional images of the PES substrate, without MBC, reveal the presence of macro-voids and short, finger-like structures within the membrane cross-section, as shown in Fig. 5 (a, b, c). The emergence of this dense structure may be due to a delayed mixing-demixing process, leading to the creation of a compact formation.

The incorporation of MBC, however, modified this pattern in relation to the substrate (Fig. 5 d, e.). All membranes that included MBC exhibited longer, more evenly dispersed finger-like structures across the substrate. The addition of hydrophilic nanofillers like MBC has been demonstrated to promote the development of a consistent finger-like structure throughout the membrane matrix by stimulating water diffusion into the polymer matrix during phase inversion [47]. When the thickness of the PES substrate exceeds a certain critical value for structural transition, macrovoids can develop, exhibiting a finger-like configuration [47,48]. The existence of this finger-like structural configuration, as compared to a sponge-like structure with nodular formations, facilitates a seamless route for water to permeate through the substrate.

In relation to the PA separating layer, incorporating MBC during the IP process leads to the formation of a uniform skin layer. This layer

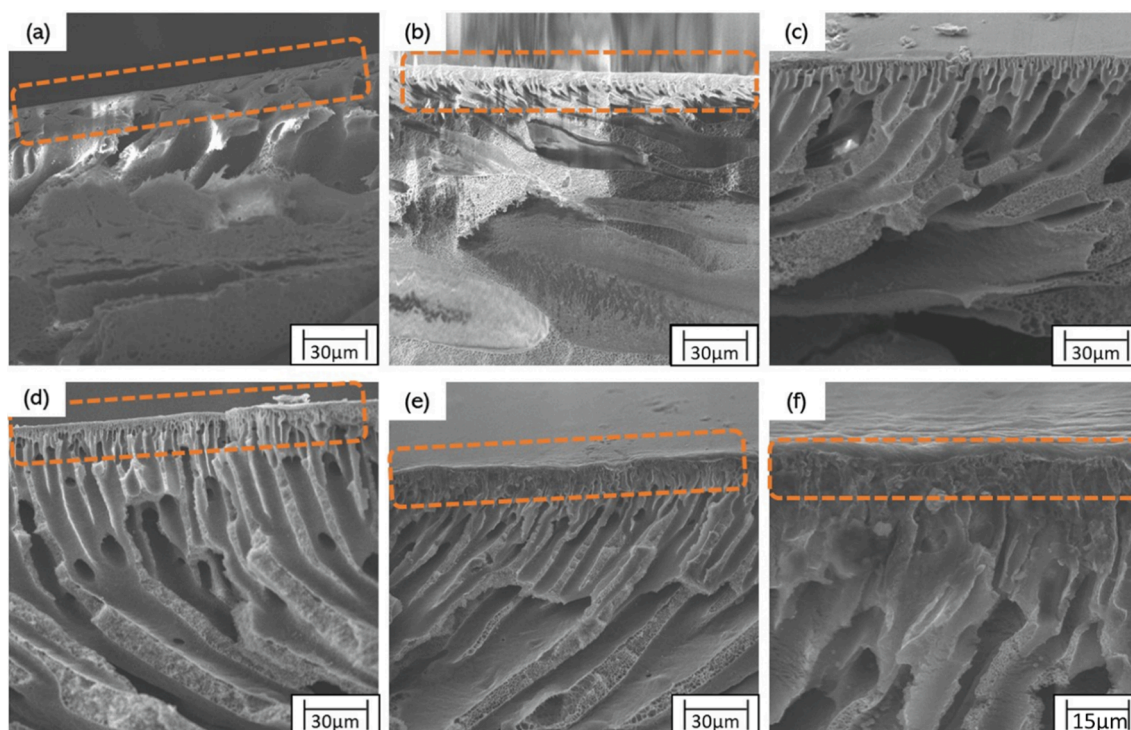


Fig. 5. Overall cross section SEM images of (a) M1, (b) M2, (c) M3, (d) M4, (e) M5 at 500x magnification, with (f) showing the selective layer of M5 which was further magnified to 2200x.

demonstrates a distinct uniformity between the PA layer and the substrate, especially in the case of the membrane with bi-metal-functionalised MBC (M5, Fig. 5, e, f). The SEM image of M5 (Fig. 5 e, f) distinctly depicts the formation of small finger-like structures in the PA separating layer. These structures progressively blend with the larger finger-like and macrovoid structures of the substrate, suggesting a high level of compatibility. The compatibility between the PA layer and substrate layer is important for both membrane stability as well as its permeation performance. Fig. 6 shows the AFM surface micrographs of all the membranes prepared in this work.

To further understand the influence of incorporating MBC into the membrane matrix, AFM analysis was carried out. In comparison to M2, M3, and M4, M5 exhibited a much higher surface roughness of 84.1 ± 11.1 nm. The presence of MBC in both the substrate and PA layer led to the formation of a more wrinkled surface region, which increases the membrane surface roughness [13]. It is a surprise to observe that the surface roughness value of M4 (MBC in substrate) is higher compared to M3 (MBC in PA layer), as it is a normal notion to expect that the presence of nanofillers on membrane surface should exhibit a higher surface roughness compared to nanofillers in the substrate region encapsulated with a PA layer [49]. This can be due to the differences in processing parameter of both the substrate and PA layer. When the casted polymer solution was immersed into a water bath, the hydrophilic properties exhibited by the MBC may lead to its movement towards the membrane surface, where phase inversion process happens. This may lead to a prominent presence of MBC on the membrane surface. PA layers without nanofillers are conformal, where they can produce thin layers with low surface roughness [50]. PA layer was prepared via IP, where the solvents were allowed to dry off in air, which could lead to the sedimentation of nanofillers into the PA layer. Nevertheless, the increase in surface roughness leads to the increment in surface area, which would be beneficial as there would be a larger effective area for water transport [51].

Fig. 7 showcases the Fourier Transform Infrared (FTIR) analysis of all the membranes fabricated in this study, spanning a range of 500 to 4000 cm^{-1} . Each membrane exhibited characteristic peaks at 1578 cm^{-1} (attributed to C=C aromatic ring stretching) and 1240 cm^{-1} (associated with aryl-O-aryl C-O stretching), both of which are derived from the PES substrate used in membrane preparation [52]. The primary PES

characteristic band at 1486 cm^{-1} (corresponding to benzene ring and C-C bond stretching) was also noticeable. The spectrum displayed an enhanced intensity in the broad-range OH functional band from 3000 to 3750 cm^{-1} with the increased incorporation of MBC into the membrane matrix (M5), in comparison to M1. This is a common observation, particularly when hydrophilic nanofillers are added to the thin selective film, as FTIR analysis is a surface-oriented analysis [53]. All membranes, except for M1, demonstrated mild peaks at 1665 and 1734 cm^{-1} , which are linked to the C-N stretching and C=O stretching vibrations, respectively. These peaks are a result of the IP process employed during the fabrication of the PA layer on the membrane surface. All the membranes that incorporated MBC also showed a peak at 2800 cm^{-1} , indicative of the aliphatic C-H bond prominent in BC.

Dynamic contact angle analysis was performed to examine the alterations in the hydrophilicity of the membrane surface after the integration of MBC. This analysis further substantiated the changes in membrane surface hydrophilicity. As depicted in Fig. 8 (a), all membranes that incorporated MBC demonstrated a lower contact angle value relative to the unmodified PES membrane, signifying an enhancement in surface hydrophilicity. M2 displayed a contact angle value around 55° , a typical range in literature, attributed to the hydrophilic acyl groups produced from the TMC used when fabricating the PA layer. Of all the samples, M5 registered the lowest contact angle value, commencing at 42.88° and reducing to 40.51° after 90 s. The improved hydrophilicity and wettability of M5 can be ascribed to the superior water affinity properties of the integrated MBC [54]. M3 recorded a lower contact angle value compared to M4 due to the placement of MBC within the membrane structure. The presence of MBC on the PA layer has a greater influence in membrane contact angle as compared to the MBC incorporated in the substrate layer [55]. However, M4 still exhibit a lower contact angle as compared to M2 even though the MBC was added in the PES substrate layer in the former while the latter does not have any MBC added in both layers. Incorporation of hydrophilic nanofillers in the substrate layer preceding the formation of PA layer can lead to improved retention of amine monomers, allowing better cross-linking with TMC and enhancing water attraction properties [56]. Furthermore, the hydroxyl and carboxylic acid functional groups present in MBC were capable of attracting water molecules through the membrane, leading to a greater surface hydrophilicity of the MBC-incorporated membranes

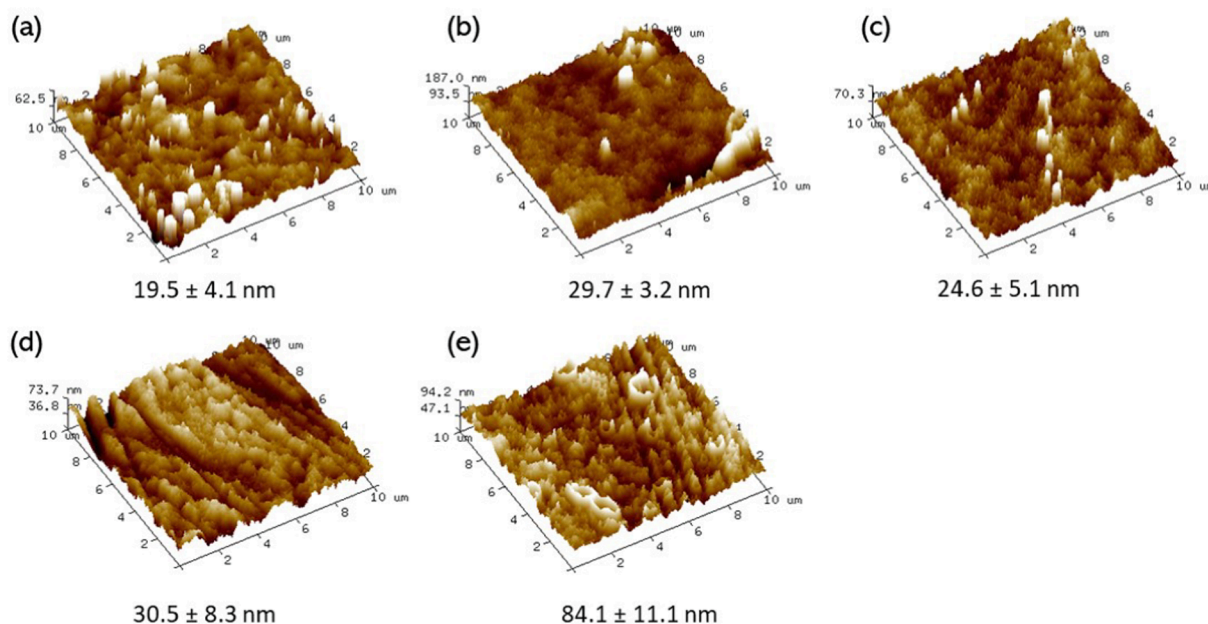


Fig. 6. Membrane surface roughness analysis for a sample size of 10 μm dimension for (a) M1, (b) M2, (c) M3, (d) M4 and (e) M5 (inset, Root Mean Square (RMS) values of each membrane).

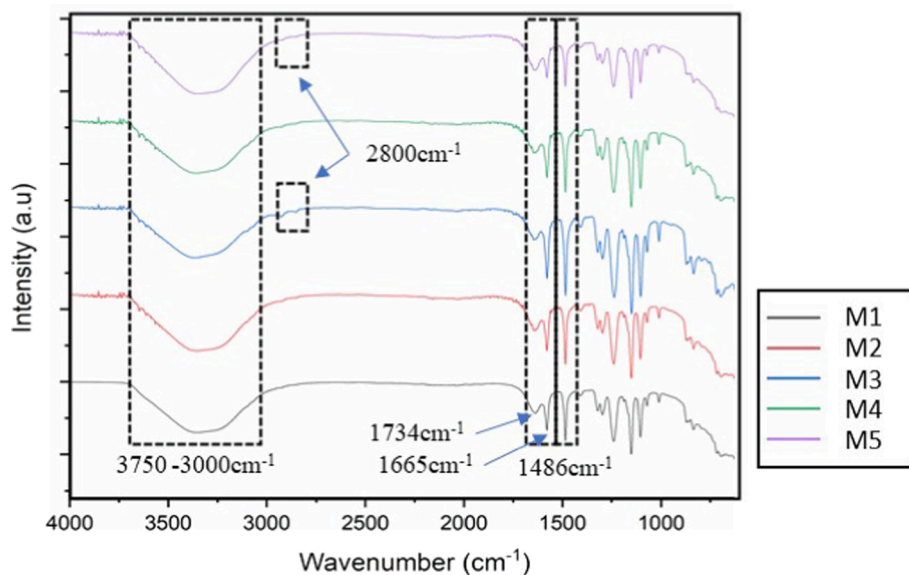


Fig. 7. FTIR analysis of M1, M2, M3, M4, M5 between 500 cm⁻¹ to 4000 cm⁻¹ at 25 °C.

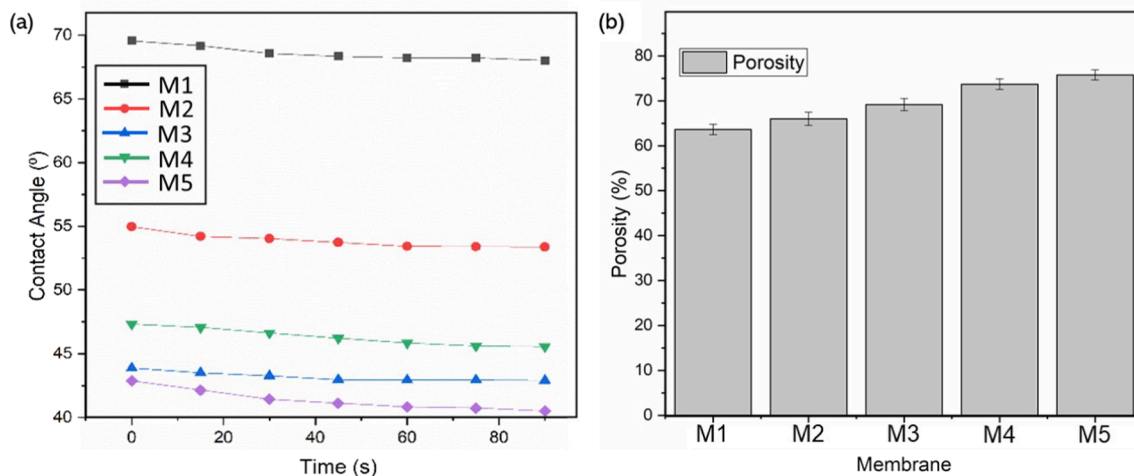


Fig. 8. (a) Dynamic surface contact angle over 90 s and (b) apparent membrane porosity of M1, M2, M3, M4 and M5.

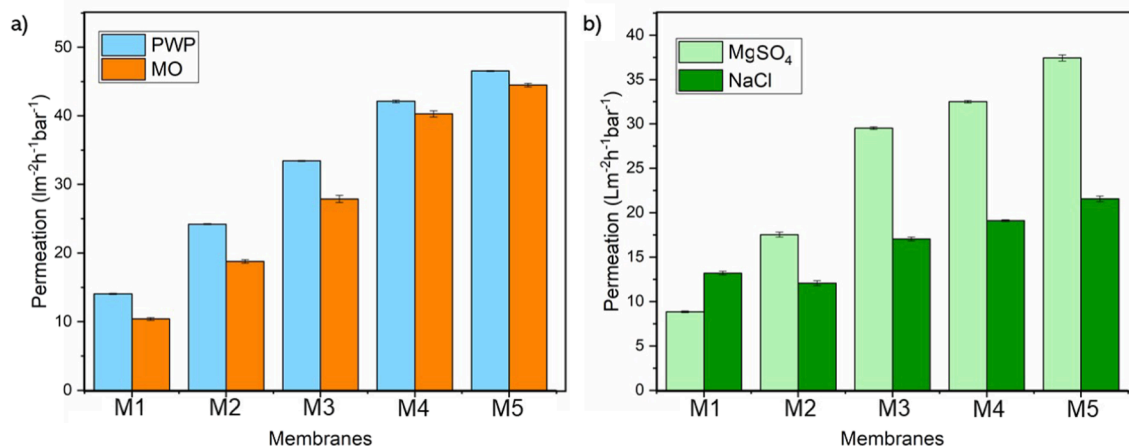


Fig. 9. (a) Permeation data for pure water and MO (10 ppm) and (b) permeation data for MgSO₄ (1000 ppm) and NaCl (1000 ppm), for membranes M1-M5.

compared to M2 [57]. The presence of hollow channels within the BC could potentially aid in the conveyance of water molecules across the membrane, functioning as nanochannels. In regard to the membrane porosity, the addition of MBC in both the PES substrate and PA layer led to M5 exhibiting the highest membrane porosity value of 75.2 %, while M2 (no MBC) exhibited a porosity value of 66.3 %. The increase in apparent porosity can be attributed to the increase in pore formation due to the delayed demixing of dope solution due to the presence of hydrophilic MBC. Furthermore, the presence of MBC in the substrate layer led to an alteration in the PES chain packing during non-solvent induced phase inversion (NIPS) [54]. Additionally, the improved hydrophilic nature of M5 compared to M2 would allow improved water retention within the membrane matrix, leading to a higher membrane porosity value for the former.

3.4. Separation performance of the membranes

The fabricated membranes underwent testing to evaluate their efficiency in separating dye and salt, as shown in Fig. 9. The tests used feed solutions with concentrations of 10 ppm for dye and 1000 ppm for salt, respectively. The observations from Fig. 9 indicate that among all the tested solutions, M5 demonstrated the highest level of water permeation, whereas M1 and M2 exhibited the lowest permeation value. M5 showed a water permeance of 46.55 ± 0.08 , 44.49 ± 0.28 , 37.43 ± 0.36 , and $21.55 \pm 0.03 \text{ Lm}^{-2}\text{h}^{-1}\text{bar}^{-1}$ for pure water, and solutions of MO, MgSO_4 , and NaCl, respectively. The enhanced permeation performance of M5, in comparison to M1 as well as M2, can be ascribed to two key factors: i) the incorporation of MBC in either substrate or PA layer enhances the hydrophilicity of the membrane, and ii) the inclusion of MBC creates additional pathways for water transport through both the selective PA layer and the PES substrate layer, resulting in accelerated permeation of water molecules across the membrane matrix. Moreover, the development of a more consistent finger-like structure throughout the membrane matrix, which is a result of the phase inversion process during the fabrication of the MMM membrane, further aids in the transport of water across the membrane matrix. The water permeation of MgSO_4 solution was higher for M2 to M5 compared to NaCl, while M1 exhibited a higher NaCl permeation compared to the former. This could be the extremely poor rejection capabilities of M1, where the porous substrate without a selective layer allowed the extremely small size of NaCl to pass through easily, without impacting the permeation performance. Comparing M3 and M4, it can be observed that the addition of MBC in the substrate PES layer was more influential in improving membrane permeation values as compared to adding them into the selective PA layer. This result is also supported with the improved membrane surface roughness as well as the water contact angle values

exhibited by M5. The addition of MBC in the PA layer played a crucial role in enhancing the selectivity of the membrane, as observed in Fig. 10.

Fig. 10 displays the rejection data for MO, MgSO_4 , and NaCl for all the membranes fabricated in this study. All membranes equipped with a PA layer exhibited a rejection of over 95 % for MO and MgSO_4 , with nearly 99 % rejection for MO. As expected, M1 demonstrated the weakest rejection performance for all tested solutions. On the other hand, M5 showed the most effective rejection performance for MO, MgSO_4 , and NaCl, with rejection rates of $99.53 \pm 0.02 \%$, $99.25 \pm 0.09 \%$, and $46.99 \pm 0.69 \%$, respectively. The rejection mechanism for all the fabricated membranes is associated with their small pore size. The molecular weight cut-off (MWCO) of a polymeric membrane dictates its capacity to separate salts based on molecular size [58]. The pore structure of the membrane selectively permits water molecules to pass through while hindering larger salt ions. This MWCO property ensures efficient separation, thereby enhancing the membrane's filtration performance in desalination processes [59]. The presence of MBC in the substrate layer plays an important role in the formation of defect free PA layer. The improved hydrophilicity of the MBC enriched PES substrate layer allows better retention of amine functional group (PIP), which in turn allows the formation of conformal and ordered PA layer when reacting with TMC during interfacial polymerisation [34,60]. In addition to this, the addition of nanomaterials into the PA layer increases its intrinsic viscosity and density as compared to PA layers without nanomaterials [61]. These features in turn enhances the selectivity of the membrane prepared. This can be observed with the slightly inhibited NaCl selectivity of M4 compared to M5. While M4 has MBC incorporated on the membrane PA layer, the NaCl selectivity is slightly lower compared to M5. While the M5 membranes demonstrated effective rejection of MgSO_4 and MO, the rejection of NaCl was relatively low, at $46.99 \pm 0.69 \%$. This implies that the molecular weight cut-off of M5 is situated between 120.37 g/mol (MgSO_4) and 58.4 g/mol (NaCl). Furthermore, Donnan's exclusion mechanism significantly contributes to polymeric membrane filtration by selectively excluding salt based on their charge. The charged characteristic of the membrane and the electrostatic repulsion between ions of similar charge inhibit the passage of salts, thereby facilitating efficient rejection. This mechanism bolsters the membrane's selectivity in solute separation during the filtration process. The elevated electronegativity of the prepared MBC, as indicated in Table 2, may enhance the surface negativity of the fabricated membrane. Consistent with the literature, the modification of membrane surface charge is observed with the minor incorporation of charged nanomaterials [62,63].

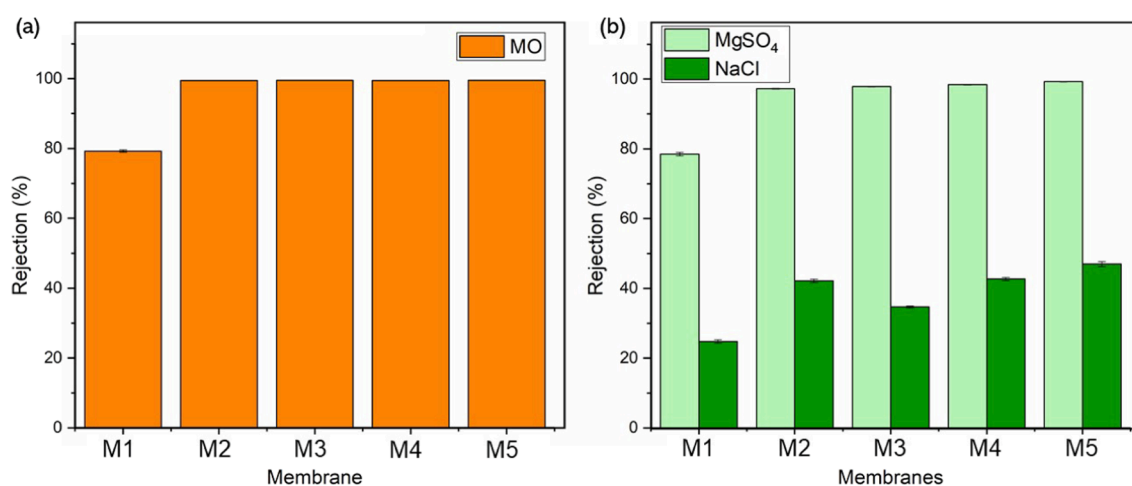


Fig. 10. (a) Rejection data of MO (10 ppm) and (b) MgSO_4 (1000 ppm) and NaCl (1000 ppm) for membranes M1-M5.

3.5. Stability tests of the M5 membrane

The stability of TFN membranes plays a pivotal role in preserving their performance across diverse applications, including water desalination and wastewater treatment. Improved durability guarantees steady and dependable operation over prolonged periods, consequently minimizing maintenance expenses and environmental footprint. This stability is also vital for attaining economic feasibility and promoting the broad-scale implementation of cutting-edge membrane technologies. In this context, the stability of the M5 membrane, in terms of rejection and permeance, was evaluated through cyclic tests, as shown in Fig. 11. Fig. 11 (a) illustrates a relatively steady rejection performance for MO, MgSO₄, and NaCl. After the third filtration cycle, there is an observed increase in the rejection of NaCl by approximately 1.5 %, which could potentially be attributed to permanent fouling. Nevertheless, the rejection of MO maintained a consistent performance, while MgSO₄ saw a slight decrease in rejection efficiency at the conclusion of each cycle. The rejection performance was reinstated following a mild cleaning of the used membranes.

In terms of permeance, the permeation of the MO solution exhibited a steady decrease, with an observed loss exceeding 10 % of the initial permeation value from the first to the last cycle. It is known that dyes can permanently bind to membranes, potentially resulting in pore blockage that cannot be eliminated through mild washing [64]. On the other hand, both MgSO₄ and NaCl demonstrated more stable permeation outcomes. Upon examining the permeation shift from cycle 3 to cycle 4 for NaCl, it was observed that the membrane could not regain its initial permeance in comparison to the preceding cycles. This observation is consistent with the noticeable increase in rejection results depicted in Fig. 11 (a).

The integration of MBC into a TFN membrane offers a promising strategy for enhancing water transport properties. BC, sourced from sustainable biomass, functions as an eco-friendly porous substrate. Metal nanoparticles, such as Fe and Zn, contribute to the increased hydrophilicity. This composite nanofiller augments the specific surface area and pore volume, thus promoting efficient water transport. The metal-functionalised BC serves as a facilitator, boosting water permeation and augmenting membrane selectivity and stability. The hydrophilicity of the metal nanoparticles amplifies their affinity for water molecules via hydrogen bonding, thereby enhancing the membrane's water permeation performance [65]. The even distribution of MBC throughout both the selective PA layer and PES substrate results in the formation of unique hydrophilic nanochannels. These channels facilitate quicker and smoother water flow, while simultaneously ensuring efficient solute retention. Furthermore, the membrane displays a well-structured design, with the presence of finger-like formations that enhance water transport. Fig. 12 illustrates how the integration of MBC

contributes to enhanced water transport while maintaining the rejection of solutes. The inclusion of MBC forms a tortuous pathway across the membrane matrix, providing additional routes for water to permeate without undermining the efficacy of salt and dye separation. The enhancement in the permeation and separation attributes of M5, when amalgamated with the nanofiller, can be chiefly credited to the nanochannels offered by the porous MBC and the amplified hydrophilicity, as corroborated by contact angle and permeation results. This innovative approach offers potential for driving advancements in the use of eco-friendly BC in water treatment membrane technologies, thereby enhancing efficiency and sustainability.

Despite the sustainable and low-carbon nature of BC, there has been minimal research undertaken on its application as a nanofiller, or as a component of a composite nanofiller, for membranes designed to improve water separation performance. Table 3 offers a comparative analysis of the performance of the M5 membrane prepared in our study, in relation to other membranes reported in existing literature for the separation of salt and organic pollutants.

The data compiled in Table 3 suggests that the performance of the membranes prepared in this study is comparable, if not superior, to those documented in the literature. While a unique aspect of this work is the integration of metals (Fe and Zn) into the BC structure. BC is naturally hydrophobic, which may limit its use as a nanofiller for water separation, as the focus of most researchers is on hydrophilic materials. However, with further processing and modification, BC produced from a myriad of sources like wheat straw, sugarcane, miscanthus, pal oil fruits and other commercial crops can be converted into an eco-friendly, hydrophilic nanofiller. This not only capitalizes on its porous structure to boost water permeation but also underscores its potential as a sustainable material. While the rejection of NaCl does not rival that of top-performing desalination membranes, M5 in this study serves as a proof of concept that BC can be utilized as an environmentally friendly and simple material in the quest for sustainable nanofillers for the creation of TFN membranes for organic pollutant removal and desalination applications.

4. Conclusion

This study has delved into the promising potential of utilizing green-derived materials, specifically BC, as distinctive nanofillers for advanced TFN membranes. The incorporation of porous MBC into a PA separating layer for TFN membrane fabrication has led to significant advancements. Imaging techniques have verified the formation of metal nanoparticles, with mapping spectra indicating a well-dispersed distribution across the porous BC substrate. Analyses of crystallinity and surface properties have unveiled a robust interaction between the metal and BC substrate, resulting in an expanded surface area and increased nanofiller

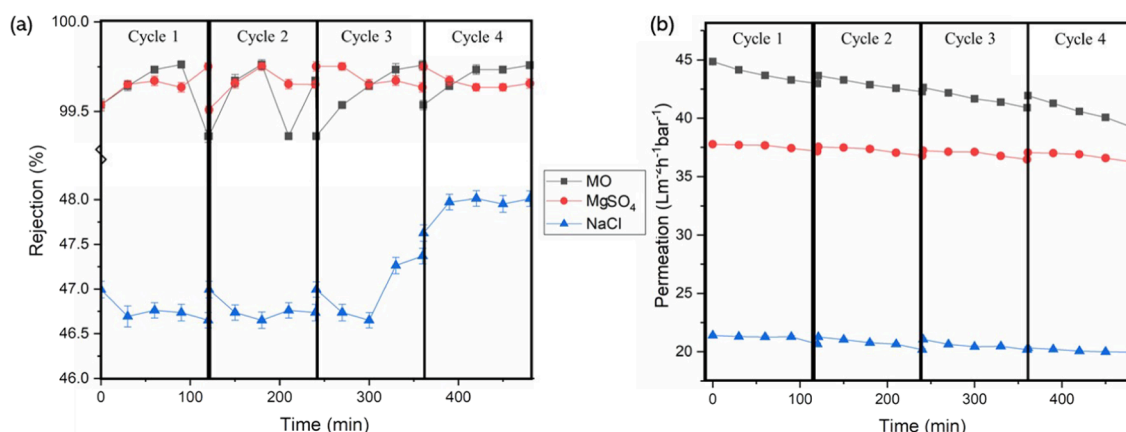


Fig. 11. (a) Cyclic rejection tests of M5 for MO, MgSO₄ and NaCl and b) cyclic permeation tests of M5 for MO, MgSO₄ and NaCl solutions.

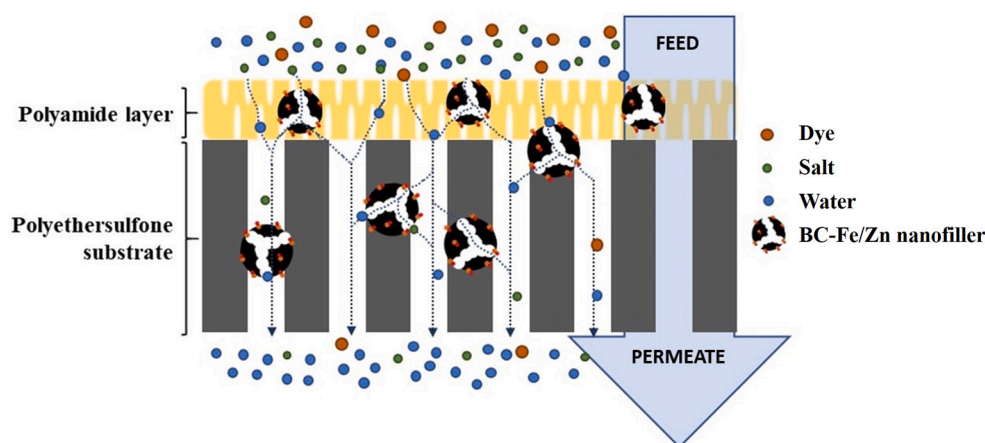


Fig. 12. Mechanisms of enhanced separation performance by the BC-Fe/Zn nanofillers.

Table 3
Comparative analysis of separation performance of BC-modified membranes.

Polymer (membrane type)	BC source	Nanofiller (loading)	PWP ($\text{Lm}^{-2}\text{h}^{-1}\text{bar}^{-1}$)	PWP Enhancement (%)	Salt rejection (%)	Rejection enhancement (%)	Organic rejection (%)	Ref.
Polydiacetylenes (PDA) (TFN)	Crayfish shell	Ball milled BC (MBC, 0.8 w/v %)	42.9	55.5	NA	30	91.10 (chlortetracycline, 100 ppm), 81.8 (Ciprofloxacin, 100 ppm) Ethanol (100 ppm)	[22]
Cellulose acetate (CA) (TFN)	Tree bark	SiO_2 @BC (0.6 w/v%)	227.00	NA	NA	NA		[66]
Polyvinylidene fluoride (PVDF) (MMM)	Wood waste	Kevlar @BC (10 wt%)	3.38	750	59.93 (NaCl, 1000 ppm), 85.37 (Na_2SO_4 , 1000 ppm)	15	95.41 (Reactive Blue 19 1000 ppm), 93.54 (Methyl blue, 1000 ppm)	[68]
Polyvinyl chloride (PVC) (MMM)	Rosmarinus officinalis leaves (RM)	RM/ZnO (15 wt%)	55.00	NA	95.00 (SO_4^{2-} , 160 ppm), 99.7 (PO_4^{3-} , 160 ppm)	47.9	NA	[23]
PES (TFN)	WS	BC-Fe/Zn (0.1 w/v%)	46.55	110	99.25 (MgSO_4 , 1000 ppm), 46.99 (NaCl, 000 ppm)	14	99.53 (MO, 10 pm)	This work

pore volume. The impacts of MBC integration in both the membrane substrate and interface layers were comprehensively examined, revealing a seamless finger-like structure across both layers, accompanied by a minor increase in surface roughness on the separating layer. Fourier transform Infra-Red (FT-IR) spectroscopy has exhibited enhanced hydrophilic functional groups on the membrane surface, as evidenced by a lower contact angle value. Permeation and rejection testing have highlighted the superiority of M5, where MBC was incorporated in both substrate and separating layers. This membrane demonstrated remarkable permeation values for water, MO, MgSO_4 , and NaCl, affirming its effectiveness in desalination applications. The rejection rates for MO, MgSO_4 , and NaCl further underscored the membrane's performance. Essentially, this work provides a compelling attempt into the application of green-derived BC, underscoring its potential for the development of TFN membranes for desalination, with an emphasis on achieving high-quality water products. The findings offer insights to the field, laying the groundwork for future advancements in sustainable and efficient membrane technologies.

CRedit authorship contribution statement

Mahesan Naidu Subramaniam: Writing – review & editing, Writing – original draft, Validation, Investigation, Formal analysis, Data curation, Conceptualization. **Shouyong Zhou:** Writing – review & editing, Resources. **Guangru Zhang:** Writing – review & editing, Resources. **Jinesh C. Manayil:** Software, Investigation, Data curation. **Zhentao Wu:** Writing – review & editing, Writing – original draft, Validation,

Supervision, Funding acquisition, Conceptualization.

Declaration of competing interest

The authors declare that they have no known competing financial interests or personal relationships that could have appeared to influence the work reported in this paper.

Data availability

Data will be made available on request.

Acknowledgements

The authors would like to acknowledge the funding support provided by The Royal Society (IEC\NSFC\201014) in the United Kingdom, State Key Laboratory of Material-Oriented Chemical Engineering (KL18-10), Leading Talents Program of Zhejiang Province (2024C03223), and the European Union Horizon 2020 Research and Innovation Program under Grant Agreement N° 862330 (INNOMEM).

References

- [1] M. Qadir, P. Drechsel, B. Jiménez Cisneros, Y. Kim, A. Pramanik, P. Mehta, O. Olaniyan, Global and regional potential of wastewater as a water, nutrient and energy source, *Nat. Resour. Forum.* 44 (2020) 40–51, <https://doi.org/10.1111/1477-8947.12187>.
- [2] K.H. Hama Aziz, F.S. Mustafa, K.M. Omer, S. Hama, R.F. Hamarawf, K.O. Rahman, Heavy metal pollution in the aquatic environment: efficient and low-cost removal

- approaches to eliminate their toxicity: a review, *RSC Adv.* 13 (2023) 17595–17610, <https://doi.org/10.1039/d3ra00723e>.
- [3] J. Jang, I. Park, S.S. Chee, J.H. Song, Y. Kang, C. Lee, W. Lee, M.H. Ham, I.S. Kim, Graphene oxide nanocomposite membrane cooperatively cross-linked by monomer and polymer overcoming the trade-off between flux and rejection in forward osmosis, *J. Memb. Sci.* 598 (2020) 117684, <https://doi.org/10.1016/j.memsci.2019.117684>.
 - [4] A. Rajput, S.K. Raj, O.V. Lebedeva, A.N. Chesnokova, T.V. Raskulova, V. Kulshrestha, Functionalized carbon dots composite cation exchange membranes: Improved electrochemical performance and salt removal efficiency, *Colloids Surf. A Physicochem. Eng. Asp.* 609 (2021) 125677, <https://doi.org/10.1016/j.colsurfa.2020.125677>.
 - [5] D.S. Dlamini, B.B. Mamba, J. Li, The role of nanoparticles in the performance of nano-enabled composite membranes – A critical scientific perspective, *Sci. Total Environ.* 656 (2019) 723–731, <https://doi.org/10.1016/j.scitotenv.2018.11.421>.
 - [6] Y. Mutharasi, N.J. Kaleekkal, T. Arumugham, F. Banat, M.S. Kapavarapu, Antifouling and photocatalytic properties of 2-D Zn/Al layered double hydroxide tailored low-pressure membranes, *Chem. Eng. Process. - Process Intensif.* 158 (2020) 108191, <https://doi.org/10.1016/j.cep.2020.108191>.
 - [7] M.R. Esfahani, S.A. Aktij, Z. Dabaghian, M.D. Firouzjaei, A. Rahimpour, J. Eke, I. C. Escobar, M. Abolhassani, L.F. Greenlee, A.R. Esfahani, A. Sadmani, N. Koutahzadeh, Nanocomposite membranes for water separation and purification: Fabrication, modification, and applications, *Sep. Purif. Technol.* 213 (2019) 465–499, <https://doi.org/10.1016/j.seppur.2018.12.050>.
 - [8] M. Asadollahi, D. Bastani, S.A. Musavi, Enhancement of surface properties and performance of reverse osmosis membranes after surface modification: A review, *Desalination* 420 (2017) 330–383, <https://doi.org/10.1016/j.desal.2017.05.027>.
 - [9] H.T. Nguyen, H.M. Bui, Y.-F. Wang, S.-J. You, Non-fluoroalkyl functionalized hydrophobic surface modifications used in membrane distillation for cheaper and more environmentally friendly applications: a mini-review, *Sustain. Chem. Pharm.* 28 (2022) 100714, <https://doi.org/10.1016/j.scp.2022.100714>.
 - [10] N. Nady, M.C.R. Franssen, H. Zuilhof, M.S.M. Eldin, R. Boom, K. Schroën, Modification methods for poly(arylsulfone) membranes: A mini-review focusing on surface modification, *Desalination* 275 (2011) 1–9, <https://doi.org/10.1016/j.desal.2011.03.010>.
 - [11] N.A. Ahmad, P.S. Goh, K.C. Wong, A.K. Zulhairun, A.F. Ismail, Enhancing desalination performance of thin film composite membrane through layer by layer assembly of oppositely charged titania nanosheet, *Desalination* 476 (2020) 114167, <https://doi.org/10.1016/j.desal.2019.114167>.
 - [12] Z. Yang, H. Guo, Z. Yao, Y. Mei, C.Y. Tang, Hydrophilic Silver Nanoparticles Induce Selective Nanochannels in Thin Film Nanocomposite Polyamide Membranes, *Environ. Sci. Technol.* 53 (2019) 5301–5308, <https://doi.org/10.1021/acs.est.9b00473>.
 - [13] G.S. Lai, W.J. Lau, P.S. Goh, A.F. Ismail, N. Yusof, Y.H. Tan, Graphene oxide incorporated thin film nanocomposite nanofiltration membrane for enhanced salt removal performance, *Desalination* 387 (2016) 14–24, <https://doi.org/10.1016/j.desal.2016.03.007>.
 - [14] Q. Wang, J. Sun, W. Xue, G. Zhao, W. Ding, K. Zhang, S. Wang, Y. Li, Effect of carbon nanotube nanochannel on the separation performance of thin-film nanocomposite (TFN) membranes, *Desalination* 546 (2023) 116216, <https://doi.org/10.1016/j.desal.2022.116216>.
 - [15] A. Zhao, N. Zhang, Q. Li, L. Zhou, H. Deng, Z. Li, Y. Wang, E. Lv, Z. Li, M. Qiao, J. Wang, Incorporation of Silver-Embedded Carbon Nanotubes Coated with Tannic Acid into Polyamide Reverse Osmosis Membranes toward High Permeability, Antifouling, and Antibacterial Properties, *ACS Sustain. Chem. Eng.* 9 (2021) 11388–11402, <https://doi.org/10.1021/acscchemeng.1c03313>.
 - [16] N.A. Mahat, S.A. Shamsudin, N. Jullok, A.H. Ma'Radzi, Carbon quantum dots embedded polysulfone membranes for antibacterial performance in the process of forward osmosis, *Desalination* 493 (2020) 114618, <https://doi.org/10.1016/j.desal.2020.114618>.
 - [17] Z. Yang, P.-F. Sun, X. Li, B. Gan, L. Wang, X. Song, H.-D. Park, C.Y. Tang, A Critical Review on Thin-Film Nanocomposite Membranes with Interlayered Structure: Mechanisms, Recent Developments, and Environmental Applications, *Environ. Sci. Technol.* 54 (2020) 15563–15583, <https://doi.org/10.1021/acs.est.0c05377>.
 - [18] C. Zhao, C. Liu, W. Wang, Z. Zhang, X. Yang, J. Tian, X. Zhang, B. Zhao, Interfacial polymerization layer with CNT providing fast water channels under electric field for efficient desalination of nanofiltration membranes, *Desalination* 565 (2023) 116825, <https://doi.org/10.1016/j.desal.2023.116825>.
 - [19] D.L. Zhao, W.S. Yeung, Q. Zhao, T.-S. Chung, Thin-film nanocomposite membranes incorporated with UiO-66-NH₂ nanoparticles for brackish water and seawater desalination, *J. Memb. Sci.* 604 (2020) 118039, <https://doi.org/10.1016/j.memsci.2020.118039>.
 - [20] A.H. Konsowa, H.Z. Abdallah, S. Nosier, M.G. Eloffy, Thin-film nanocomposite forward osmosis membrane for water desalination: synthesis, characterization and performance improvement, *Water Qual. Res. J.* 57 (2022) 72–90, <https://doi.org/10.2166/wqrj.2022.034>.
 - [21] P. Jagnade, N.L. Panwar, T. Gupta, C. Agrawal, Role of Biochar in Agriculture to Enhance Crop Productivity: An Overview, *Biointerface Res, Appl. Chem.* 13 (2023), <https://doi.org/10.33263/BRIAC135.429>.
 - [22] D. Zhang, K. Zhang, X. Hu, Y. Xue, L. Zhang, Y. Sun, Ball-milled biochar incorporated polydopamine thin-film composite (PDA/TFC) membrane for high-flux separation of tetracycline antibiotics from wastewater, *Sep. Purif. Technol.* 272 (2021) 118957, <https://doi.org/10.1016/j.seppur.2021.118957>.
 - [23] R. Mohammadi, M. Hezarjaribi, D.L. Ramasamy, M. Sillanpää, A. Pihlajamäki, Application of a novel biochar adsorbent and membrane to the selective separation of phosphate from phosphate-rich wastewaters, *Chem. Eng. J.* 407 (2021) 126494, <https://doi.org/10.1016/j.cej.2020.126494>.
 - [24] M. Armezardiz Ontiveros, Y. Quintero, A. Llanquilef, M. Morel, L. Argente Martnez, A. Garcia Garcia, A. Garcia, Anti-Biofouling and Desalination Properties of Thin Film Composite Reverse Osmosis Membranes Modified with Copper and Iron Nanoparticles, *Materials (basel)* 12 (2019), <https://doi.org/10.3390/ma12132081>.
 - [25] N. Ghaemi, S.S. Madaeni, P. Daraei, H. Rajabi, S. Zinadini, A. Alizadeh, R. Heydari, M. Beygzadeh, S. Ghouzivand, Polyethersulfone membrane enhanced with iron oxide nanoparticles for copper removal from water: Application of new functionalized Fe₃O₄ nanoparticles, *Chem. Eng. J.* 263 (2015) 101–112, <https://doi.org/10.1016/j.cej.2014.10.103>.
 - [26] J. Leichtweis, S. Silvestri, N. Welter, Y. Vieira, P.I. Zaragoza-Sánchez, A.C. Chávez-Mejía, E. Carissimi, Wastewater containing emerging contaminants treated by residues from the brewing industry based on biochar as a new CuFe₂O₄ / biochar photocatalyst, *Process Saf. Environ. Prot.* 150 (2021) 497–509, <https://doi.org/10.1016/j.psep.2021.04.041>.
 - [27] M.B. Nguyen, G.H. Le, T.D. Nguyen, Q.K. Nguyen, T.T.T. Pham, T. Lee, T.A. Vu, Bimetallic Ag-Zn-BTC/GO composite as highly efficient photocatalyst in the photocatalytic degradation of reactive yellow 145 dye in water, *J. Hazard. Mater.* 420 (2021) 126560, <https://doi.org/10.1016/j.jhazmat.2021.126560>.
 - [28] M.N. Subramaniam, P.S. Goh, W.J. Lau, M.N.Z. Abidin, S. Mansur, B.C. Ng, A. F. Ismail, Optimizing the spinning parameter of titania nanotube-boron incorporated PVDF dual-layered hollow fiber membrane for synthetic AT-POME treatment, *J. Water Process Eng.* 36 (2020), <https://doi.org/10.1016/j.jwpe.2020.101372>.
 - [29] Y. Zhao, Y. Liao, G.S. Lai, Y. Yin, R. Wang, A tight polyethersulfone ultrafiltration membrane fabricated via polyion complex assisted phase inversion for dye desalination, *J. Memb. Sci.* 685 (2023) 121908, <https://doi.org/10.1016/j.memsci.2023.121908>.
 - [30] M.N. Subramaniam, P.S. Goh, W.J. Lau, B.C. Ng, A.F. Ismail, AT-POME colour removal through photocatalytic submerged filtration using antifouling PVDF-TNT nanocomposite membrane, *Sep. Purif. Technol.* 191 (2018) 266–275, <https://doi.org/10.1016/j.seppur.2017.09.042>.
 - [31] E.K. Motlagh, S. Sharifian, N. Asasian-kolur, Bioresource Technology Reports Alkaline activating agents for activation of rice husk biochar and simultaneous bio-silica extraction, *Bioresour. Technol. Reports.* 16 (2021) 100853, <https://doi.org/10.1016/j.biteb.2021.100853>.
 - [32] C. Liu, W. Wang, R. Wu, Y. Liu, X. Lin, H. Kan, Y. Zheng, Preparation of Acid- and Alkali-Modified Biochar for Removal of Methylene Blue Pigment, *ACS Omega* 5 (2020) 30906–30922, <https://doi.org/10.1021/acsomega.0c03688>.
 - [33] L.I. Trakhtenberg, M.I. Ikim, O.J. Ilegbusi, V.F. Gromov, G.N. Gerasimov, Effect of Nanoparticle Interaction on Structural, Conducting and Sensing Properties of Mixed Metal Oxides, *Chemosensors* 11 (2023), <https://doi.org/10.3390/chemosensors11060320>.
 - [34] G.S. Lai, W.J. Lau, P.S. Goh, M. Karaman, M. Gürsoy, A.F. Ismail, Development of thin film nanocomposite membrane incorporated with plasma enhanced chemical vapor deposition-modified hydrous manganese oxide for nanofiltration process, *Compos. Part B Eng.* 176 (2019) 107328, <https://doi.org/10.1016/j.compositesb.2019.107328>.
 - [35] T. van den Berg, M. Ulbricht, Polymer nanocomposite ultrafiltration membranes: The influence of polymeric additive, dispersion quality and particle modification on the integration of zinc oxide nanoparticles into polyvinylidene difluoride membranes, *Membranes (basel)* 10 (2020) 1–19, <https://doi.org/10.3390/membranes10090197>.
 - [36] X. Li, C. Jiao, X. Zhang, Z. Tian, X. Xu, F. Liang, G. Wang, H. Jiang, A general strategy for fabricating polymer/nanofiller composite membranes with enhanced CO₂/N₂ separation performance, *J. Clean. Prod.* 350 (2022) 131468, <https://doi.org/10.1016/j.jclepro.2022.131468>.
 - [37] A.-A.M. Helmy, E.-A.E. Zakaria, B. Mohamed, A.-H.A. Farouk, F.E. M., A.-H.S.M. S., Z.M. Shafick, DFT and experimental study on adsorption of dyes on activated carbon prepared from apple leaves, *Carbon Lett.* 31 (2021) 863–878, [10.1007/s42823-020-00187-1](https://doi.org/10.1007/s42823-020-00187-1).
 - [38] E. Pusceddu, S.F. Santilli, G. Fioravanti, A. Montanaro, F. Miglietta, P.U. Foscolo, Chemical-physical analysis and exfoliation of biochar-carbon matter: From agriculture soil improver to starting material for advanced nanotechnology, *Mater. Res. Express.* 6 (2019), <https://doi.org/10.1088/2053-1591/ab4ba8>.
 - [39] M. Geça, A.M. Khalil, M. Tang, A.K. Bhakta, Y. Snoussi, P. Nowicki, M. Wiśniewska, M.M. Chehimi, Surface treatment of biochar—methods surface analysis and potential applications: a comprehensive review, *Surfaces* 6 (2023) 179–213, <https://doi.org/10.3390/surfaces6020013>.
 - [40] L. Wang, Z. Li, G. Mao, Y. Zhang, F.P. Lai, Effect of Nanoparticle Adsorption on the Pore Structure of a Coalbed Methane Reservoir: A Laboratory Experimental Study, *ACS Omega* 7 (2022) 6261–6270, <https://doi.org/10.1021/acsomega.1c06770>.
 - [41] A. Rabajczyk, M. Zielecka, K. Cygańczuk, Ł. Pastuszka, L. Jurecki, Nanometals-Containing Polymeric Membranes for Purification Processes, *Mater. (basel, Switzerland)* 14 (2021), <https://doi.org/10.3390/ma14030513>.
 - [42] S. Noamani, S. Niroomand, M. Rastgar, M. Sadrzadeh, Carbon-based polymer nanocomposite membranes for oily wastewater treatment, *npj Clean Water* 2 (2019) 1–14, <https://doi.org/10.1038/s41545-019-0044-z>.
 - [43] S. Mallakpour, E. Khadem, Carbon nanotube-metal oxide nanocomposites: Fabrication, properties and applications, *Chem. Eng. J.* 302 (2016) 344–367, <https://doi.org/10.1016/j.cej.2016.05.038>.
 - [44] A.M.A. Abdelsamad, M. Matthias, A.S.G. Khalil, M. Ulbricht, Nanofillers dissolution as a crucial challenge for the performance stability of thin-film

- nanocomposite desalination membranes, *Sep. Purif. Technol.* 228 (2019) 115767, <https://doi.org/10.1016/j.seppur.2019.115767>.
- [45] G.S. Lai, W.J. Lau, S.R. Gray, T. Matsuura, R. Jamshidi Gohari, M.N. Subramaniam, S.O. Lai, C.S. Ong, A.F. Ismail, D. Emazadah, M. Ghanbari, A practical approach to synthesize polyamide thin film nanocomposite (TFN) membranes with improved separation properties for water/wastewater treatment, *J. Mater. Chem. a* 4 (2016) 4134–4144, <https://doi.org/10.1039/c5ta09252c>.
- [46] N.S. Lazarenko, V.V. Golovakhin, A.A. Shestakov, N.I. Lapekin, A.G. Bannov, Recent Advances on Membranes for Water Purification Based on Carbon Nanomaterials, *Membranes (basel)* 12 (2022), <https://doi.org/10.3390/membranes12100915>.
- [47] X. Wu, T.M. Kohl, J. Tsanaksidis, Z. Xie, Improved Performance and Mitigated Internal Concentration Polarization of Thin-Film Composite Forward Osmosis Membrane with Polysulfone/Polyaniline Substrate, *ACS Appl. Polym. Mater.* 3 (2021) 5758–5766, <https://doi.org/10.1021/acsapm.1c00964>.
- [48] C.-S. Lin, K.-L. Tung, Y.-L. Lin, C.-D. Dong, C.-W. Chen, C.-H. Wu, Fabrication and modification of forward osmosis membranes by using graphene oxide for dye rejection and sludge concentration, *Process Saf. Environ. Prot.* 144 (2020) 225–235, <https://doi.org/10.1016/j.psep.2020.07.007>.
- [49] L.A. Perry, N.G.P. Chew, K. Grzebyk, P. Cay-Durgun, M.L. Lind, P. Sitaula, M. Soukri, O. Coronell, Correlating the role of nanofillers with active layer properties and performance of thin-film nanocomposite membranes, *Desalination* 550 (2023) 116370, <https://doi.org/10.1016/j.desal.2023.116370>.
- [50] Y.S. Khoo, W.J. Lau, Y.Y. Liang, N. Yusof, A. Fauzi Ismail, Surface modification of PA layer of TFC membranes: Does it effective for performance Improvement? *J. Ind. Eng. Chem.* 102 (2021) 271–292, <https://doi.org/10.1016/j.jiec.2021.07.006>.
- [51] J. Chen, Y. bai, E. Nabil Shokry Gadallah, X. Xu, Y. Jing, M. Lou, X. Zhang, F. Li, Enhancing the perm-selectivity of thin-film nanocomposite membranes intercalated with cyclodextrin-chelated Metal-Organic Framework via modulated interfacial polymerization, *J. Memb. Sci.* 693 (2024) 122382, <https://doi.org/10.1016/j.memsci.2023.122382>.
- [52] F. Behdarvand, E. Valamohammadi, M.A. Tofighy, T. Mohammadi, Polyvinyl alcohol/polyethersulfone thin-film nanocomposite membranes with carbon nanomaterials incorporated in substrate for water treatment, *J. Environ. Chem. Eng.* 9 (2021) 104650, <https://doi.org/10.1016/j.jece.2020.104650>.
- [53] M.H. Tajuddin, N. Yusof, I. Wan Azelee, W.N. Wan Salleh, A.F. Ismail, J. Jaafar, F. Aziz, K. Nagai, N.F. Razali, Development of copper-aluminum layered double hydroxide in thin film nanocomposite nanofiltration membrane for water purification process, *Front. Chem.* 7 (2019) 1–11, <https://doi.org/10.3389/fchem.2019.00003>.
- [54] S.A. Kumar, G. Srinivasan, S. Govindaradjane, A novel synergistic effect of TiO₂ and ZnO incorporation in PES-based thin-film nanocomposite nanofiltration membrane for treatment of textile wastewater, *Environ. Monit. Assess.* 194 (2022), <https://doi.org/10.1007/s10661-022-10525-7>.
- [55] S.R. Razavi, A. Shakeri, H. Mahdavi, Polymer-Grafted Graphene Oxide as a High-Performance Nanofiller for Modification of Forward Osmosis Membrane Substrates, *ACS Appl. Polym. Mater.* 4 (2022) 8878–8891, <https://doi.org/10.1021/acsapm.2c01266>.
- [56] G.S. Lai, W.J. Lau, P.S. Goh, Y.H. Tan, B.C. Ng, A.F. Ismail, A novel interfacial polymerization approach towards synthesis of graphene oxide-incorporated thin film nanocomposite membrane with improved surface properties, *Arab. J. Chem.* 12 (2019) 75–87, <https://doi.org/10.1016/j.arabjc.2017.12.009>.
- [57] T. Sun, L. Wang, R. Hu, Y. Li, Z. Zhu, Light controls edge functional groups to enhance membrane permeability, *Front. Phys.* 11 (2023) 1–7, <https://doi.org/10.3389/fphy.2023.1098170>.
- [58] M. Borpatra Gohain, S. Karki, D. Yadav, A. Yadav, N.R. Thakare, S. Hazarika, H. K. Lee, P.G. Ingole, Development of Antifouling Thin-Film Composite/Nanocomposite Membranes for Removal of Phosphate and Malachite Green Dye, *Membranes (basel)* 12 (2022), <https://doi.org/10.3390/membranes12080768>.
- [59] S. Homaeigohar, M. Elbahri, Graphene membranes for water desalination, *NPG Asia Mater.* 9 (2017) 1–16, <https://doi.org/10.1038/AM.2017.135>.
- [60] R. Dai, Z. Yang, Z. Qiu, L. Long, C.Y. Tang, Z. Wang, Distinct impact of substrate hydrophilicity on performance and structure of TFC NF and RO polyamide membranes, *J. Memb. Sci.* 662 (2022) 120966, <https://doi.org/10.1016/j.memsci.2022.120966>.
- [61] M.N. Subramaniam, P.S. Goh, Y.H. Tan, S.J. Chiong, W.J. Lau, B.C. Ng, A.F. Ismail, J.Y. Chuah, S.O. Lai, Antifouling Improvement of Polyethersulfone Membrane Incorporated with Negatively Charged Zinc-Iron Oxide for AT-POME Colour Removal, *Arab. J. Sci. Eng.* 44 (2019) 5571–5580, <https://doi.org/10.1007/s13369-019-03858-y>.
- [62] B.-M. Jun, J. Cho, A. Jang, K. Chon, P. Westerhoff, Y. Yoon, H. Rho, Charge characteristics (surface charge vs. zeta potential) of membrane surfaces to assess the salt rejection behavior of nanofiltration membranes, *Sep. Purif. Technol.* 247 (2020) 117026, <https://doi.org/10.1016/j.seppur.2020.117026>.
- [63] P. Kumar, U.G. Thummar, N.H. Nandha, P.S. Singh, Sustainable treatment of saline dye wastewater and resource recovery with flux-recoverable hollow fiber of antifouling ‘water channel’, *Desalination* 549 (2023) 116308 <https://doi.org/10.1016/j.desal.2022.116308>.
- [64] A.E.D. Mahmoud, E. Mostafa, Nanofiltration Membranes for the Removal of Heavy Metals from Aqueous Solutions, *Prepar. Appl. Membr. (basel)* 13 (2023), <https://doi.org/10.3390/membranes13090789>.
- [65] Y. Lan, N. Yan, W. Wang, Polydimethylsiloxane (PDMS) membrane filled with biochar core-shell particles for removing ethanol from water, *BioResources*. 12 (2017) 6591–6606. [10.15376/biores.12.3.6591-6606](https://doi.org/10.15376/biores.12.3.6591-6606).
- [66] S. Gu, L. Li, F. Liu, J. Li, Biochar/Kevlar nanofiber mixed matrix nanofiltration membranes with enhanced dye/salt separation performance, *Membranes (basel)*. 11 (2021), <https://doi.org/10.3390/membranes11060443>.